Shape Optimization and Numerical Modeling of Precast Hollow Core Panels for External Walls in Multi-story Buildings

Rajenthirakumar Subakaran[a], Thishan Jayasinghe[a], Sumudu Herath[a,*]

[a] *Department of Civil Engineering, University of Moratuwa, Bandaranayake Mawatha, Moratuwa 10400, Sri Lanka*

Abstract

During the past decade, precast wall panels became one of the popular precast panel elements satisfying both load-bearing and non-load bearing structural requirements. Originally, precast wall panels were intended to be used as internal partition wall panels, which are not expected to resist loading nor undergo significant deformations. This paper focuses on verifying the usability of such precast panels as external wall panels in multi-story buildings, where their load resistance is investigated under lateral wind loads and vertical deformations due to column shortening effects. In addition, using the shape optimization technique in-built into ABAQUS advanced finite element software, a better layout for the precast wall is also proposed and its performance is compared with the current standard layout under similar loading and boundary conditions. It is shown that the optimized design has a higher load-bearing capacity and does not impose any challenges in manufacturing. Using shape optimized panel sections, panel assemblies are simulated to investigate the panel assembly response under wind loads. Further, recommendations are given on the maximum number of wall panels that could be installed as a single assembly under different wind load intensities at various heights of multi-story buildings. Considering practical aspects, these recommendations are integrated with proposals on connection mechanisms between panel assemblies.

Keywords: precast wall panels, shape optimization, numerical modeling, multi-story buildings, hollow core panels, optimal layout

1. Introduction

1.1. Background

Due to the increasing population and reduced availability of usable lands for construction activities, many residential and commercial buildings are becoming medium- to high-rise structures globally. Complementing this trend, the global construction industry has incorporated precast products as core elements due to their better performance, enhanced quality, elevated control, reduced leading time of construction, adaptability of novel technologies in

*Corresponding author
Email address: sumuduh@uom.lk (Sumudu Herath)

Preprint submitted to Elsevier *Received: date / Accepted: date*

construction and controlled material processing during manufacturing. Currently, 50% of the global 7.9 billion population has claimed major cities as their residences, while it is estimated that it will be increased to 67% by 2050 [1]. In this growing population, providing standard living facilities will be a foreseen challenge. According to Kumar et.al [2], in a case study based in India, the necessity to build housing facilities is at a rate of 30 to 35 thousand housing units per day for the next 8 years. Similarly, in a very short period, Hong Kong has experienced a massive residential building demand. In Hong Kong, massive housing projects were initiated during the 1950s to tackle the demand and it is continuing to date [3]. On the other hand, infrastructure development projects play a major role in the economic growth of countries, especially developing countries. The most common challenges faced during the construction phase of any project in developing countries are cost overruns and schedule delays. In a case study conducted in a low-income country, the average delay in a construction project was found to be 143%, with a maximum and minimum of 802% and 9% respectively. Evidently, such delays in construction projects can cause adverse impacts on all related stakeholders and it is important to look for solutions to mitigate such known impacts [4].

For this work, the construction industry of Sri Lanka is chosen to furnish the contextual background. The capital cost of construction has increased exponentially during the last decade in Sri Lanka, as the material prices are inflated due to the increased demand for construction projects, skilled and unskilled labor deficits along with the reduced supply of quality materials [5]. Apart from the resource constraints, global warming, which has become a major threat to the sustainability of the globe, has significantly restricted the expansion of construction industries as major policymakers are now encouraging greener practices in engineering [6]. In concrete-based constructions, cement is responsible for the CO_2 emissions from the production phase until the end of the construction phase. According to Ibrahim et.al [6], the production of one ton of Portland cement contributes to one ton of CO_2 emission directly and indirectly. Hence, the effective ways in which these carbon footprints can be reduced are now a global concern in every industry. In the civil engineering industry, sustainable practices have evolved, marking various milestones such as; carbon fiber reinforced concrete [7], natural fiber reinforced concrete [8], additive manufacturing of concrete [9], self-compacting concrete [10], precast concrete [11, 12, 13].

Precast wall panels are carefully engineered structures that have shown notable time savings in construction projects [14, 15, 16, 17, 18, 19]. In general, precast elements are designed and manufactured under a controlled environment and passed through several testing and quality inspections before being transported to the respective construction sites. This ensures the expected quality of the final structural outputs in comparison to the in-situ concrete constructions. In addition, precast elements can easily be geometrically parameterized, and hence are shaped flexible and geometrically very precisely. Specifically, precast wall panels can be categorized into two distinct divisions serving two different purposes. The first is the exterior cladding. These behave as an interface between the interior space and exterior space. Claddings only transfer lateral loads to the structural frame. The other one is the structural load-bearing walls. These resist combinations of shear, flexure, and axial loads. These are manufactured in the forms of solid panels, hollow-core panels, insulated panels, ribbed and architectural panels [20].

1.2. Related Work

Several studies have been conducted to determine the usability of the precast wall elements in building constructions [21]. The panel-to-panel connections of such wall panels are crucial for the structural integrity of the construction. Vaghei et.al [22] experimentally tested and modeled the connection between two wall panels using horizontal steel hooks embedded into the walls. Other research studies were focused on evaluating the structural performance of wall panels with openings using the Finite Element Method (FEM) [1], the structural integrity of precast wall panels under seismic load [6, 23, 24], assessing the damage in precast concrete wall panel connections under blast loading using finite element analysis [25], and shear behavior of two-way hollow-core wall panels [26]. However, most of these research works are focused entirely to investigate several characteristics of reinforced concrete or pre-stressed concrete wall panels, but none of them was focused to investigate the usability of plain concrete wall panels to be used in multi-story buildings. In a research study conducted by Diaz et al. [27], hollow core masonry blocks were modeled and several core shapes were analyzed using ANSYS commercial finite element software to obtain an optimal hollow core masonry block to be used in automated assembly constructions.

1.3. Precast Hollow Core Panels

The Precast Hollow Core Wall Panels (PHCWPs) considered in this research study are manufactured in Sri Lanka by the International Construction Consortium (Pvt) Ltd (ICC). According to ICC-ACOTEC Precast Wall Panels Technical & Installation Manual [28], three different cross-section designs are manufactured presently, and they are as listed in Table 1. For this research study, a panel with 140mm thickness was chosen. The presented numerical studies could be directly employed in the rest of the panels similarly. Further, a brief discussion on the panel installation process is outlined below. For a detailed technical discussion please refer to the Installation Manual [28].

Table 1: Hollow core panel geometries (ICC-ACOTEC) [28]

Thickness (mm)	**Length (mm)**	**Width (mm)**
75 ± 3	2700	600 ± 5
100 ± 3	3300	600 ± 5
140 ± 3	3300	600 ± 5

The PHCWPs are attached to the columns by three pieces of 10 mm dowels. These dowels can be connected to columns using ICC-ACOTEC grout. Figure 1 shows the connection between a column and a panel [28].

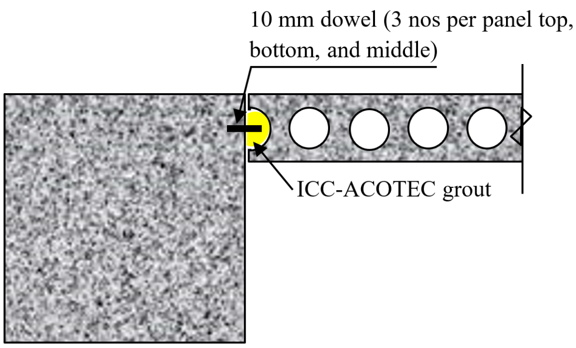

Figure 1: Panel to Column connection using dowel and grouting

Each PHCWP is connected with the aid of an interlocking tongue and groove. After the panels are positioned in place, the joints are grouted, and the seams are taped with crack control tape [28]. The tongue and groove of the panels are shown in Figure 2.

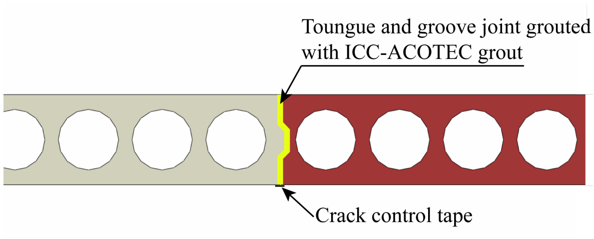

Figure 2: Tongue and groove connection between panels

A U-shaped steel bracket is used to connect the PHCWP at its top and bottom to respective concrete beams (see Figure 3). The panels are erected such that the steel brackets are in line with the cores of the panel. Figure 3 shows the steel U bracket, modeled using AutoCAD 3D.

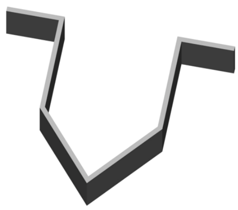

Figure 3: U-shaped steel bracket for top and bottom connection

2. Numerical modeling of PHCWPs

2.1. Geometric modeling of PHCWPs

ABAQUS/CAE advanced element (FE) software is used extensively in this research. This choice is evident based on similar past research works by Mohamed et.al [29], Risan et.al [30], and Joda et.al [1]. Especially, the Concrete Damage Plasticity (CDP) material model available in ABAQUS/CAE inspired the same choice. Note that in this paper, ABAQUS/CAE commands are denoted by an asterisk (*) as a prefix to a particular keyword.

The cross-section of the chosen panel for this research study, of dimensions 140 mm x 600 mm, is shown in Figure 4.

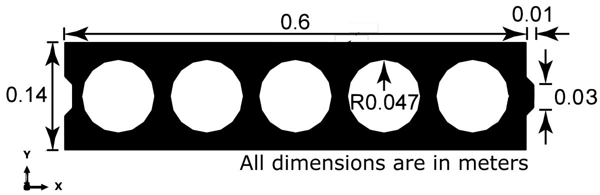

Figure 4: Section geometry of the 140 mm x 600 mm panel with five circular cores of an internal radius of 47 mm. Dimensions are

A solid homogeneous section was chosen for the panel's numerical analysis in ABAQUS. Further, 8-node linear solid elements having reduced integration with hourglass control (Q3D8R) were used to discretize the panel and the element deletion was manually enabled using the command *ELEMENT DELETION=YES. The 3D view of the panel is shown in Figure 5.

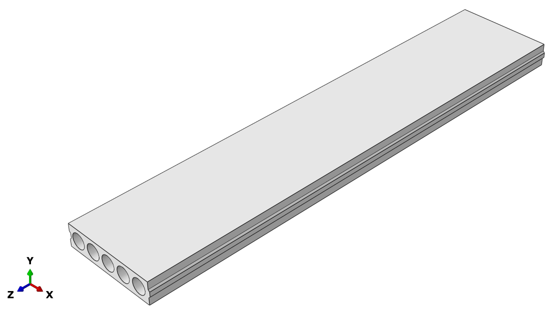

Figure 5: 3D view of the 140mm x 600mm panel modeled in ABAQUS/CAE

2.2. Concrete Damage Plasticity (CDP) Model

CDP is one of the accurate representative constitutive models of concrete. CDP model captures both concrete crushing and cracking mechanisms and has been widely used in many research works [31, 32, 33]. According to the ABAQUS user manual [34], the parameters that are required to define the plasticity of concrete are; dilation angle (ψ), eccentricity of concrete, σ_{b0}/σ_{c0} ratio, viscosity parameter, and yield shape surface (κ). The recommended values of these parameters are given in Table 2.

Table 2: CDP parameters used in the study

Parameter	Recommended Value
Dilation angle	30° - 40°
Eccentricity	0.1
σ_{b0}/σ_{c0}	1.16
κ	2/3
Viscosity parameter	0.0

The compressive and tensile behaviors of concrete are defined in ABAQUS modeling in terms of yield stress, inelastic strain and cracking strain [34]. To determine these parameters Stress-Strain variation of concrete in both tension and compression is required. Upon the non-availability of experimental results of concrete used in manufacturing PHCWPs, the compressive behavior is obtained using the mathematical model provided in the Eurocode EN 1992-1-1 [35]. Subsequently, the tensile behavior is calculated using the mathematical model produced by Wang & Hsu [36]. Moreover, though the dilation angle can take a value within 30° - 40° [34], the optimal dilation angle for a similar application is obtained as 35° [32]. Hence in this study, the dilation angle is considered as 35°.

The compressive stress-strain values for concrete are calculated according to Eurocode EN 1992-1-1 [35] using equation (1).

$$\frac{\sigma_c}{f_{cm}} = \frac{\kappa\eta - \eta^2}{1 + (\kappa - 2)\eta} \tag{1}$$

where

$\eta = \frac{\epsilon_c}{\epsilon_{c1}}$

ϵ_{c1} is the strain at peak stress

$\kappa = 1.05 E_{cm} \times |\epsilon_{c1}|/f_{cm}$

f_{cm} is the mean value of concrete cylinder strength

E_{cm} is the secant modulus of elasticity of concrete

Eurocode EN 1992-1-1 proposes several numerical relationships in idealizing the concrete tensile behavior, incorporating the tension stiffening effects [36, 37, 38, 39]. Herein, the tensile stress-strain behavior for the analyses was calculated using Equations (2) and (3).

$$\sigma_1 = E_c \epsilon_1 \qquad \epsilon_1 \leq \epsilon_{cr} \tag{2}$$

$$\sigma_1 = f_{cr} \frac{\epsilon_{cr}}{\epsilon_1} \qquad \epsilon_1 > \epsilon_{cr} \tag{3}$$

where

E_c is the modulus of elasticity

ϵ_{cr} is the cracking strain of concrete

f_{cr} is the cracking stress of concrete

The Stress-Strain relationship calculated following the above-mentioned mathematical models for concrete of ultimate strength 15 MPa is depicted in Figure 6.

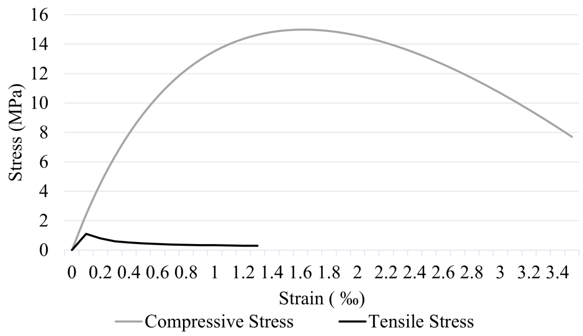

Figure 6: Stress-strain variation of the concrete used in this study

CDP modeling in ABAQUS requires Yield stress, damage parameter in both compression, and tension, inelastic strain for compression and cracking strain for tension as user inputs [34]. The compression and tension damage parameters are calculated according to Equation (4).

$$\begin{cases} d_c &= 1 - \frac{\sigma_c}{\sigma_{cu}} \\ d_t &= 1 - \frac{\sigma_t}{\sigma_{t0}} \end{cases} \tag{4}$$

For the calculation of inelastic and cracking strains, elastic strain in both compression and tension is required. These parameters are calculated using Equation (5) and the inelastic and cracking strain are calculated using Equation (6).

$$\begin{cases} \epsilon_{oc}^{el} &= \frac{\sigma_c}{E_0} \\ \epsilon_{ot}^{el} &= \frac{\sigma_t}{E_0} \end{cases} \tag{5}$$

$$\begin{cases} \epsilon_{\mathrm{c}}^{\mathrm{in}} &= \epsilon_0 - \epsilon_{0\mathrm{c}}^{\mathrm{el}} \\ \epsilon_{\mathrm{t}}^{\mathrm{in}} &= \epsilon_0 - \epsilon_{0\mathrm{t}}^{\mathrm{el}} \end{cases} \tag{6}$$

2.3. *Failure identification in ABAQUS/CAE*

The panel was modeled in ABAQUS/CAE, and two reference points were established on the top (RP_TOP) and the bottom (RP_BTM) surfaces' geometric center. Each of these surfaces was connected using rigid body constraint to the respective reference points. The bottom reference point was given a fixed boundary condition and the top reference point was applied with a uniformly increasing displacement to simulate displacement-controlled uniaxial compression test. Before running the model, damage in compression (DAMAGEC) and damage in tension (DAMAGET) were explicitly requested in the field output. DAMAGEC and DAMAGET will show the approximate crushing and cracking positions in the panel. Since the element deletion was turned on as mentioned in Section 2.1, the elements that underwent crushing or cracking will be removed from the domain. The applied boundary condition and loading along with the panel is shown in Figure 7.

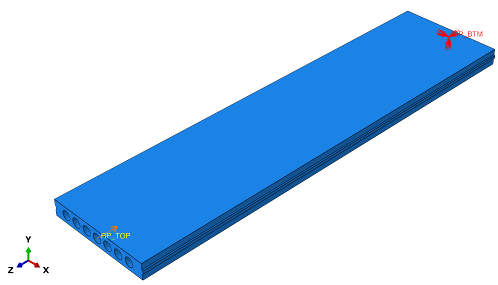

Figure 7: Applied boundary condition along with the uniformly increasing displacement loading in the panel

2.4. *Model validation*

As common to any finite element based numerical studies, it is important to perform a mesh sensitivity analysis to find the optimal compromise between mesh size (density) and computational cost. Hence, a mesh convergence study is conducted by varying mesh densities and recording the corresponding failure load. Six sets of different mesh sizes are used in this study and the results are presented in Figure 8.

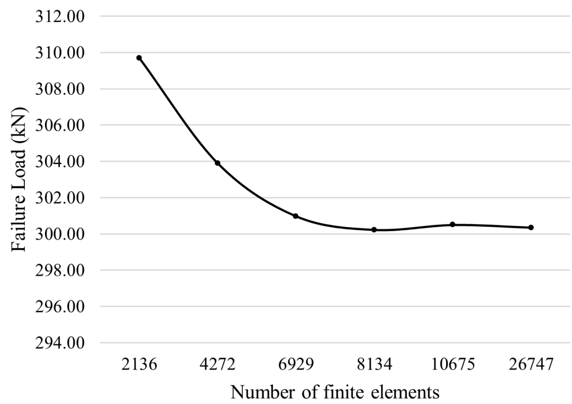

Figure 8: Failure load variation with mesh density represented in terms of the number of finite elements in the model

As evident from Figure 8, failure load converges to approximately 300 kN in the presence of minimum of 8134 finite elements. Considering the computational time, which was about 17.58 minutes on a Core i7 2.8 GHz processor with 16 gigabytes of memory, as well as the numerical accuracy (see Figure 8), a finite element mesh having 10675 elements is chosen in subsequent analyses.

The concrete properties of the PHCWPs used in this study were not known. Therefore, experiments were conducted to arrive at the material properties of concrete. Herein, experimental results of the Uniaxial Compression Loading (UCL) and four-point flexural test for PHCWPs were used to determine the material properties. Initially, several grades of concrete were chosen and the required material properties were calculated as mentioned in section 2.1. Several UCL were simulated using ABAQUS/CAE for the calculated material properties. The failure loads obtained for each grade of concrete were compared with the failure load obtained from the experiments. The variation of failure load for different grades of concrete is shown in Figure 9 and a typical failure pattern of a panel (of concrete strength 7 MPa) is shown in Figure 10.

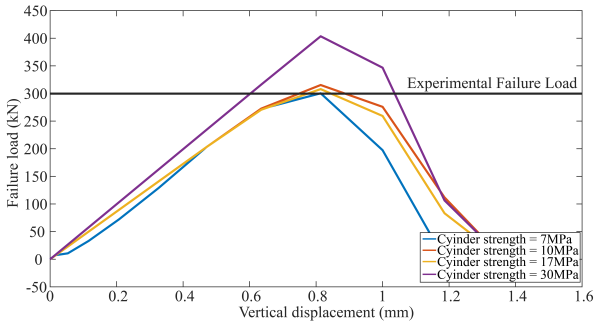

Figure 9: Failure loads for the panels of concrete cylinder strengths 7 MPa, 10 MPa, 17 MPa, and 30 MPa under uniaxial compression loading

The grade of concrete which gave a failure load that is closer to the experimental result was taken for subsequent analyses. This nearest concrete cylinder strength was recorded as 7 MPa (see Figure 10). The equivalent panel failure stress was obtained as 1.09 MPa while the applied vertical displacement on the panel during the failure was recorded as 0.81375 mm. It is highlighted that the panel failure (at 300 kN) was due to excessive tensile stresses induced due to panel bending during the UCL. To validate this independently, a four-point flexural test was also simulated. The failure stress of the numerical four-point flexural test arrived as 1.084 MPa which is in good agreement with the previous numerical results. Stress distribution (S33) of the panel under the 4-point loading test at the failure load is shown in Figure 11. Therefore, using the panel experimental results, numerical models were validated and respective CDP model parameters are calibrated. The validated material properties are given in Table 3.

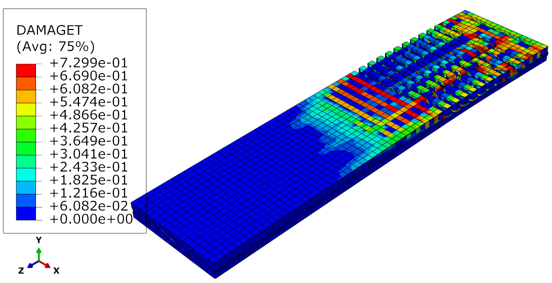

Figure 10: Failure pattern of a panel of concrete cylinder strength 7 MPa under UCL

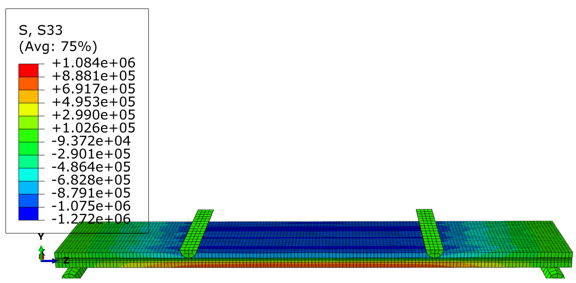

Figure 11: Longitudinal stress variation of the panel under 4-point flexural test

Table 3: Concrete material properties: measured and validated from numerical analyses

Material Property	**Magnitude**
Density	1885 kgm^{-3}
Mean cylinder strength (f_{cm})	15 MPa
Cube strength ($f_{ck,cube}$)	8.75 MPa
Mean axial tensile strength (f_{ctm})	1.1 MPa
Secant modulus (E_{cm})	25 GPa
Poisson's ratio	0.2
Dilation angle	35°

2.5. Interaction definition between two interlocking panels

Now the focus is rendered towards the numerical modeling of the panel assembly. The edges along with the tongue and groove connection were constrained using tie constraints in ABAQUS/CAE. This moment-transferable structural idealization is justified by the high-strength grout that holds to panels at the connecting edges (see Figure 2). Fixing the panel's bottom edge, to simulate the connection of a panel with the slab beneath, would cause early failure of the panels, as shown in Figure 12. This is evident because of the higher bending moments developed near the bottom edge of the panel. Therefore, the bottom edge is modeled as a pinned boundary. In other words, the grout is assumed to be cracked along the bottom under the lateral loading conditions. Later in this research study, a channel section was proposed to hold the panels and these panels are assumed to have only a frictional contact (thus structurally less important)

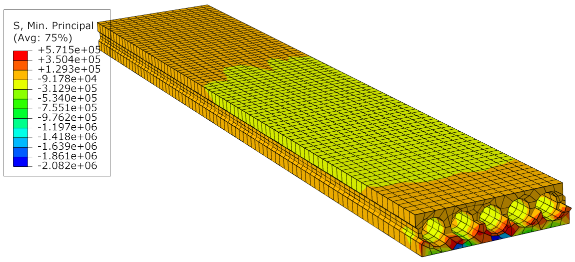

Figure 12: Premature failure of the panel due to maximum bending moment along the bottom edge

between the proposed channel section. Assuming small displacements and to reduce model complexities, the channel section was not modeled alongside the panel. Therefore, the vertical edges of a panel assembly are idealized as pinned connections. The applied boundary conditions in the ABAQUS modeling are shown in Figure 13.

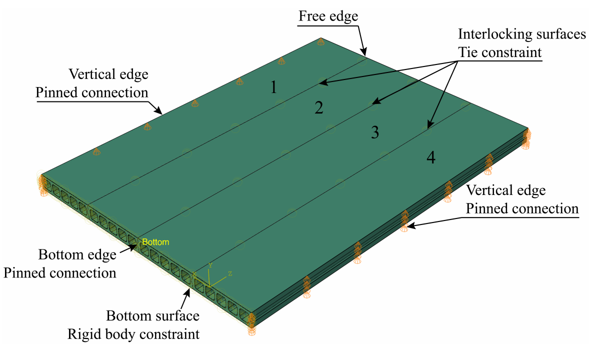

Figure 13: An assembly of four panels with three exterior edges modeled as pinned connection, top as free edge, and interlocks as tie constraints

3. Shape optimization of PHCWPs

3.1. Shape Optimization of Solids

Shape optimization is one of the three structural optimizations techniques (topology, shape, and size) that is widely used in both academic and industrial research tasks [40, 41]. Shape optimization focuses on optimizing the geometric boundary of a structure to improve structural performance by reducing stress concentrations [42]. Non-optimal response of circular hollow sections upon fatigue loading is one of the lessons learned after the tragic de Havilland Comet's Failure [43]. In general, a shape optimization process involves minimizing a convex objective function (e.g. such as the compliance) subjected to pre-defined constraints (e.g. such as thickness, volume, or displacement bounds) [44]. The optimization solver built-in ABAQUS/CAE requires defining the design domain and design responses. The design domain is the region of the panel where the optimization is defined, and design responses are panel-related quantities such as weight, volume, damage, or contact stress [34].

In this research study, the design regions are the hollow core areas, which are defined using *DV_SHAPE. The geometric constraints are the exterior boundary surfaces of the panels, defined using *DVCON_SHAPE. Two design responses are defined namely, the strain energy and volume of the design domain using the ABAQUS command *DRESP. 60% of the retention volume (volume fraction) of the panel was selected as the initial volume constraint and the objective function (*OBJ_FUNC) was set to minimize the strain energy density. Further, all boundary surfaces of PHCWPs were frozen so that those regions will not be optimized because those areas contain the tongue and grooves as well as the wall surfaces (see Figures 4 and 5).

3.2. Shape optimal PHCWPs

For a single PHCWP, the above-mentioned shape optimization process was carried out. A lateral load of 1500 Pa was applied on the vertical surface of the panel. Moreover, the same panel is pinned along the bottom edge to restrict rigid body translations and rotations. The optimized shape of the panel cores is shown in Figure 14. Herein, for better visualization, a mid-depth cut of the pre- and post- optimized panel is presented.

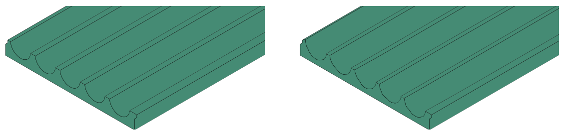

(a) (b)

Figure 14: (a) Pre-optimization and (b) post-optimization shapes of the hollow cores

The inherent weakness of ABAQUS optimization solver is its inability to produce Computer Aided Design (CAD) models of the optimal design [40]. Hence, an iterative manual geometry tuning process was used to obtain an easy-to-manufacture geometry that can be utilized in an extrusion-based manufacturing process. The optimal core design revealed that the use of a squircle for the cores will lead to the best stress distribution in the vicinity of cores. This cross-section is depicted in Figure 15. The fillet radius was found using a localized sensitivity analysis using values between 5 - 50 mm which agrees with the shape optimal design shown in Figure 14b. The best stress distribution was attained when the fillet radius is taken as 10 mm. Further, the proposed cross-section uses 19.88% less concrete volume than that of the original panel shown in Figure 4. This reduced volume in the proposed design, however, does not reduce its compressive strength capacity in comparison to the original panel. This shape optimal design is used in the subsequent analyses of this research study.

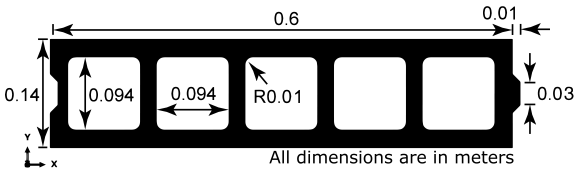

Figure 15: Selected section geometry for the hollow-core panel

4. PHCWP assemblies in Multi-story Buildings

4.1. Use of PHCWPs in multi-story buildings

Load-bearing wall panels are expected not only to withstand shear forces, bending moments, and axial forces but also to maintain stability between the neighboring panels or structural frame [20]. As a result, inevitable axial shortening is observed in multi-story buildings due to long-term creep and shrinkage effects [45]. According to Ali et.al [46], the maximum column shortenings that can be expected in a 12-story and a 24-story building could be as high as 27.1 mm and 151.6 mm, respectively. In the UCL simulation done in this research work, the panels fail under a vertical displacement of slightly less than 1 mm. Therefore, plain (non-reinforced) concrete wall panels are not recommended to be used in buildings as load-bearing structural elements, where significant axial shortening can be expected. This conclusion is evident as plain concrete has near-zero tensile strength to resist bending stresses arising due to loading eccentricities. To circumvent this challenge, there are studies carried out in the recent past to check the performance of reinforced concrete wall panels against several loading conditions [47, 48, 49, 50, 51]. In this study, we have considered the response of plain concrete panel assemblies in the presence of axial shortening and lateral loading. To this end, the shape optimal designs of the panel sections are used in the simulations of panel assemblies.

4.2. Numerical Simulation of PHCWP assemblies in multi-story buildings

It was shown earlier in Section 2.4 that PHCWP failed under an axial vertical displacement of around 1 mm (see Figure 9). Also, as the scope of the study is concentrated on external walls in multi-story buildings, the panels are next analyzed under lateral wind loads. A 30-story building with a footprint of 30 m x 42 m was considered for the wind load calculations. Per the Eurocode EN 1991-1-1-4:2005 [52] and its National counterpart SLS EN 1991-1-4: 2019 [53], a maximum wind load of 1.402 kPa on the 30$^{\text{th}}$ floor is attained. For wind load calculations, the parameters tabulated in Table 4 were used.

Table 4: Wind load related parameters of a 30-story (109 m tall) building of plan dimension 30 m x 42 m

Parameter	**Value**	**Reference**
V_b,map	23 m/s	SLS EN 1991-1-4:2019 Appendix 1 [53]
b	30 m	
d	42 m	
h	109 m	
Z_0	0.3 m	EN Table 4.1 [52]
Z_{min}	5 m	EN Table 4.1 [52]
Z_e	10 m	Figure 7.4 [53]
V_b	23 m/s	SLS EN 4.2 (2)P Note 1 [53]
$C_r(z)$	1.271756	Equation 4.4
V_m	29.25 m/s	Equation 4.3
$I_v(z)$	0.1694	Equation 4.7
q_p	1168.7 Pa	Equation 4.8
h/d	2.6	Figure 7.5
$C_{pe,10}$	1.2	Table 7.1
W_e	1402.4 Pa	Equation 5.1

To this end, panel assemblies having 3, 4, 5 and 6 panels were modelled with the interactions detailed in Section 2.5. Initially, a wind load of 2 kPa was applied on all panel assemblies. This value of 2 kPa (> 1.402 kPa) is selected to present the expected failure of an assembly. Therein, a typical failure of the assembly having 6-panels is shown in Figure 16. Subsequently, A lateral wind load of 1.5 kPa was applied on the same 6-panel assembly and the panel barely withstood this wind load. Minor tension cracks are observed along the core edges (see Figure 17), but the assembly as a whole did not fail. The maximum displacement of the panel in the lateral direction was 0.93 mm as shown in Figure 17.

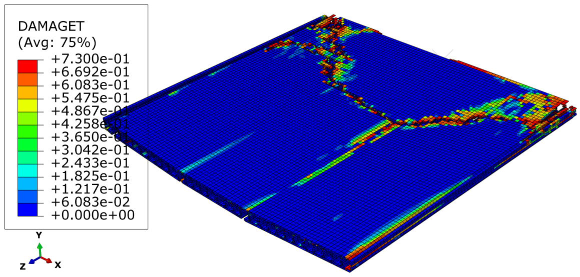

Figure 16: 6-panel assembly failure pattern under 2 kPa lateral wind load

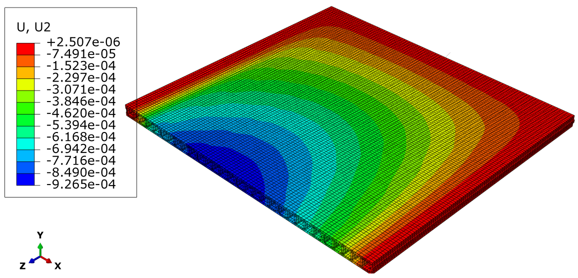

Figure 17: 6-panel assembly under 1.5 kPa lateral wind load

When the lateral wind load was increased to 2 kPa (taking a partial safety factor 1.4 on loading), the 6-panel assembly failed, whereas the 3, 4, 5-panel assemblies withstood without any tension damage. The maximum lateral displacement observed in the 5-panel assembly was 0.22 mm and the lateral displacement variation of the same is shown in Figure 18.

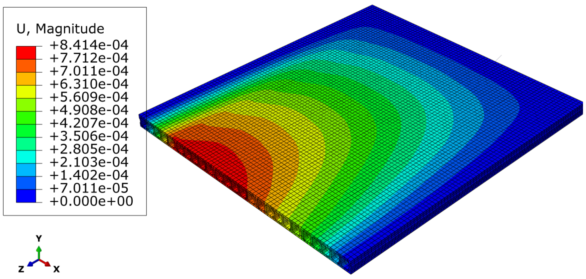

Figure 18: 5-panel assembly under 2 kPa lateral wind load

According to the above analysis, it is evident that 5-panel assemblies can be safely installed in multi-story buildings having up to 30 stories in the wind zone 3 of Sri Lanka. Using the same numerical approach, the following recommendations are made at different heights of buildings located in different wind zones of Sri Lanka. Separate analyses for 3, 4, 5, and 6-panel assemblies at different wind loads were conducted in coming up with the recommendations given in Figure 19.

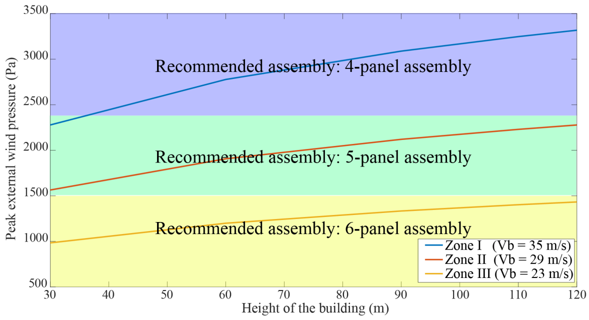

Figure 19: Recommendations of panel assemblies for various wind pressures (at different building heights) in wind zones I, II, and III of Sri Lanka.

4.3. Panel assembly installation - Practical considerations

Wall panels considered in this study have a fixed width of 600 mm (see Table 1). Thus, ignoring the thickness of the grout in between the panels, 5 and 6-panel assemblies will have maximum assembly widths of 3 m and 3.6 m respectively. However, the clear distance between two adjacent columns is generally more than 3.6 m. Taking a 6-panel assembly as an example, several assemblies of the same will be required during the installation. To circumvent this problem, a new connection mechanism is proposed to hold the panel assemblies in place and provide structural support. A steel channel section (C-section) is proposed, such that it will support the panels along the vertical edges on both sides of an assembly. The internal width of the C-section is selected as the panel thickness plus a working tolerance of 3 mm on each side (see Table 1). The proposed channel sections holding a 3-panel assembly are shown in Figure 20. Furthermore, the arrangement of 3-panel assemblies adjacent to each other is shown in Figure 21.

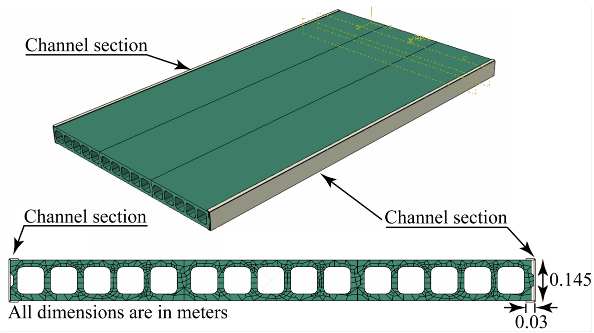

Figure 20: Proposed connection details of the panel assembly; 3D view (top) and section view (bottom)

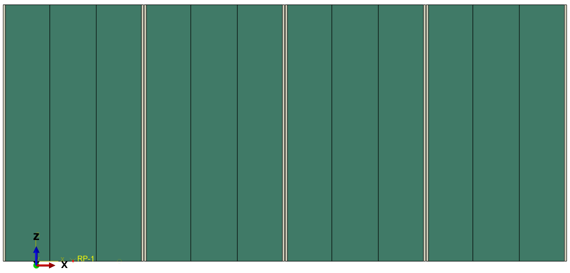

Figure 21: Arrangement of four 3-panel assemblies between two columns

The proposed S275 structural steel channel section has an internal width of 146 mm, 10 mm web thickness and 5 mm flange thickness. This was numerically modelled and verified using ABAQUS/CAE. The most critical loading scenario was considered when the panel assembly is supported only along the vertical edges by two channel sections which are fixed at the bottom. This panel arrangement leads to a one-way spanning simply supported wall panel. The load that will act on the channel sections of height 3.3 m, when the 5-panel assembly is acted by a wind load of 1.5 kPa, is calculated and applied as a uniformly distributed load. From the numerical analysis, the maximum Von-misses stress observed in the channel section was 50 MPa and the maximum displacement was 9.324 mm. For structural steel of grade S275 and a span of 3.3 m, these results are satisfactory [54]. However, the fatigue strength of the proposed channel section should be evaluated prior to installation, as cyclic wind loads could lead to fatigue failure of the same. Fatigue strength evaluation is not considered within the scope of this work. f

5. Limitations and Future Directions

The presented numerical study has a limited scope with regard to the type of panels considered. Out of the three options given in Table 1, this paper presented a detailed and rigorous numerical investigation of a single panel. However, to make recommendations similar to Figure 19, one can use the same methodology presented in this paper. Further, long-term effects such as creep and fatigue need to be incorporated into the numerical study to understand the panel behavior during the service time of a multi-story building. Tunable (or parametric) shape optimal design of hollow core panels could be an interesting future work in terms of areal topology and size optimization.

6. Conclusions

In this research study, the structural response of hollow core panels against lateral wind loads and axial shortening effects were studied. The selected hollow core panel for simulations, with section dimension 140 mm x 600 mm, was first subjected to axial compressive (uni-axial compressive loading - UCL) and flexural (four-point bending) tests for model validation against experimental results. After model calibration, the same panel was subjected to shape optimization. At this juncture, panel's section geometry was modified iteratively, such that it has the same strength but a 19.88% lower volume than that of the original section. This readily-manufacturable shape optimal design is used in the subsequent structural analyses. 3-, 4-, 5- and 6-panel assemblies were simulated for various wind load intensities (in each wind zone) expected at different heights of a multi-story building. Herein, the assembly capacity of each panel assembly was attained. Figure 19 summarizes these findings. For instance, when the wind load is below 1.5 kPa, shape-optimized panel assemblies having 6-panels can be utilized in a single assembly. Moreover, guidance on practical considerations was discussed. For example, adequate clearance should be provided between the panels and the beam bottom to prevent any excessive stress generation due to column shortenings. It was numerical analyzed and subsequently proposed to use an S275 steel channel section to hold the panel assemblies in place along the vertical edges while the panel bottoms are supported by the slab (or beam). It is advised to incorporate slotted holes for the proposed channel sections in the vicinity of a column to accommodate column shortening.

References

[1] Saad Abdulqader Ali Joda, Abdul Aziz Abdul Samad, and Noridah Mohamed. Numerical analysis of precast wall panels with openings. *International Journal of Sustainable Construction Engineering and Technology*, 11(2):30–41, 2020.

[2] Ram Kumar, Manoj Patterson, and Sandeep Jain. A case study on use of precast technology for construction of high-rise buildings. *NTPC Global Energy Technology Summit (GETS)*, 2016.

[3] Lara Jaillon and Colleen S Poon. The evolution of prefabricated residential building systems in hong kong: A review of the public and the private sector. *Automation in construction*, 18(3):239–248, 2009.

[4] Solomon Melaku Belay, Seifu Tilahun, Mitiku Yehualaw, Jose Matos, Helder Sousa, and Endalew Temesgen Workneh. Analysis of cost overrun and schedule delays of infrastructure projects in low income economies: Case studies in ethiopia. *Advances in Civil Engineering*, 2021, 2021.

[5] JMSN Jayasooriya and TD Denagama. Comparative analysis of precast construction and conventional construction of small-scale concrete building in terms of cost.

[6] M Ibrahim, MK Rahman, LM AlHems, and M Maslehuddin. Structural performance of innovative precast hollow concrete walls for buildings.

[7] Zhihong Zheng and Dorel Feldman. Synthetic fibre-reinforced concrete. *Progress in Polymer Science*, 20(2):185–210, 1995.

[8] M Fan and F Fu. Introduction: A perspective–natural fibre composites in construction. In *Advanced high strength natural fibre composites in construction*, pages 1–20. Elsevier, 2017.

[9] Freek Bos, Rob Wolfs, Zeeshan Ahmed, and Theo Salet. Additive manufacturing of concrete in construction: potentials and challenges of 3d concrete printing. *Virtual and physical prototyping*, 11(3):209–225, 2016.

[10] PL Domone. Self-compacting concrete: An analysis of 11 years of case studies. *Cement and concrete composites*, 28(2):197–208, 2006.

[11] PE Amin Einea, David Salmon, Gyula J Fogarasi, Todd D Culp, and Maher K Tadros. State-of-the-art of precast concrete sandwich panels. *PCI journal*, 36(6):78–98, 1991.

[12] Alfred A Yee and PE Hon D Eng. Social and environmental benefits of precast concrete technology. *PCI journal*, 46(3):14–19, 2001.

[13] Alfred A Yee and PE Hon D Eng. Structural and economic benefits of precast/prestressed concrete construc-

tion. *PCI journal*, 46(4):34–43, 2001.

[14] Svetlana Brzev and Teresa Guevara-Perez. Precast concrete construction. *Canada: British Columbia Institute of Technology, Canada*, 2010.

[15] Abraham Warszawski, Moshe Avraham, and David Carmel. Utilization of precast concrete elements in building. *Journal of construction engineering and management*, 110(4):476–485, 1984.

[16] AL kulabi Ahmed and Hakob Avetisyan. Reducing time and cost of construction projects by improving the properties of precast normal-weight wall panels. *Procedia engineering*, 145:1066–1073, 2016.

[17] P Karthigai Priya and M Neamitha. A review on precast concrete. *International Journal of Engineering and Technology (IRJET)*, 5(1), 2018.

[18] Ragavendra Holla, Siddhant Anant, Muzzamil Ali Muhammad, Aakash Periwal, and Aakash Kapoor. Time, cost, productivity and quality analysis of precast concrete system. *International Journal of Innovative Science, engineering and technology*, 3(5):252–257, 2016.

[19] Shubham Singhal, Ajay Chourasia, Yogesh Kajale, and Dirgha Singh. Behaviour of precast reinforced concrete structural wall systems subjected to in-plane lateral loading. *Engineering Structures*, 241:112474, 2021.

[20] David Ragan et al. Behavior of efficient two story precast concrete wall panels. 2011.

[21] Sidney Freedman. Loadbearing architectural precast concrete wall panels. *PCI journal*, 44(5):92–115, 1999.

[22] Ramin Vaghei, Farzad Hejazi, Hafez Taheri, Mohd Saleh Jaafar, and Abang Abdullah Abang Ali. Evaluate performance of precast concrete wall to wall connection. *APCBEE procedia*, 9:285–290, 2014.

[23] Rodrigo Lameiras, Joaquim AO Barros, Isabel B Valente, Elisa Poletti, Matilde Azevedo, and Miguel Azenha. Seismic behaviour of precast sandwich wall panels of steel fibre reinforced concrete layers and fibre reinforced polymer connectors. *Engineering Structures*, 237:112149, 2021.

[24] John L Wilson, Angela J Robinson, and T Balendra. Performance of precast concrete load-bearing panel structures in regions of low to moderate seismicity. *Engineering Structures*, 30(7):1831–1841, 2008.

[25] Azer Maazoun, John Vantomme, and Stijn Matthys. Damage assessment of hollow core reinforced and prestressed concrete slabs subjected to blast loading. *Procedia engineering*, 199:2476–2481, 2017.

[26] Chen Xiong, Mingjin Chu, Jiliang Liu, and Zhijuan Sun. Shear behavior of precast concrete wall structure based on two-way hollow-core precast panels. *Engineering Structures*, 176:74–89, 2018.

[27] JJ del Coz Díaz, PJ García Nieto, FP Álvarez Rabanal, and A Lozano Martínez-Luengas. Design and shape optimization of a new type of hollow concrete masonry block using the finite element method. *Engineering Structures*, 33(1):1–9, 2011.

[28] *ICC-ACOTEC Precast Wall Panel Technical and Installation Manual*. International Construction Consortium Pvt Ltd, Sri Lanka, 2018.

[29] Zohreh Asaee, Mbarka Mohamed, Sadman Soumik, and Farid Taheri. Experimental and numerical characterization of delamination buckling behavior of a new class of gnp-reinforced 3d fiber-metal laminates. *Thin-Walled Structures*, 112:208–216, 2017.

[30] Hussam K Risan, Ibrahim SI Harba, and Abdulkhalik J Abdulridha. Numerical analysis of rc wall with opening strengthened by cfrp subjected to eccentric loads. *Graevinar*, 69(07.):573–580, 2017.

[31] Ali Raza, Afaq Ahmad, et al. Numerical investigation of load-carrying capacity of gfrp-reinforced rectangular concrete members using cdp model in abaqus. *Advances in Civil Engineering*, 2019, 2019.

[32] Adam Wosatko, Andrzej Winnicki, Maria Anna Polak, and Jerzy Pamin. Role of dilatancy angle in plasticity-based models of concrete. *Archives of Civil and Mechanical Engineering*, 19(4):1268–1283, 2019.

[33] Liming Jiang, M Anwar Orabi, Jian Jiang, and Asif Usmani. Modelling concrete slabs subjected to fires using

nonlinear layered shell elements and concrete damage-plasticity material. *Engineering Structures*, 234:111977, 2021.

[34] Michael Smith. *ABAQUS/Standard User's Guide*. Dassault Systèmes Simulia Corp, United States, 2020.

[35] EN 1992-1. *Eurocode 2: Design of concrete structures - Part 1-1: General rules and rules for buildings*. European Committee for Standardization, London, 2004.

[36] Taijun Wang and Thomas TC Hsu. Nonlinear finite element analysis of concrete structures using new constitutive models. *Computers & structures*, 79(32):2781–2791, 2001.

[37] Milad Hafezolghorani, Farzad Hejazi, Ramin Vaghei, Mohd Saleh Bin Jaafar, and Keyhan Karimzade. Simplified damage plasticity model for concrete. *Structural Engineering International*, 27(1):68–78, 2017.

[38] Buddhi Wahalathantri, David Thambiratnam, Tommy Chan, and Sabrina Fawzia. A material model for flexural crack simulation in reinforced concrete elements using abaqus. In *Proceedings of the first international conference on engineering, designing and developing the built environment for sustainable wellbeing*, pages 260–264. Queensland University of Technology, 2011.

[39] David W Murray, Chung Wong, Khazal Y Rijub-Agha, and Larp Chitnuyanondh. Concrete plasticity theory for biaxial stress analysis. *Journal of the Engineering Mechanics Division*, 105(6):989–1006, 1979.

[40] Sumudu Herath and Udith Haputhanthri. Topologically optimal design and failure prediction using conditional generative adversarial networks. *International Journal for Numerical Methods in Engineering*, 122:6867–6887, 12 2021.

[41] Sumudu Herath, Udith Haputhanthri, and Chinthaka Mallikarachchi. Initial design of trusses using topology optimization in a deep learning environment. In *2020 From Innovation to Impact (FITI)*, volume 1, pages 1–6, 2020.

[42] Raphael T Haftka and Ramana V Grandhi. Structural shape optimization—a survey. *Computer methods in applied mechanics and engineering*, 57(1):91–106, 1986.

[43] P. A. Withey. Fatigue failure of the de Havilland comet I. *Engineering Failure Analysis*, 4(2):147–154, jun 1997.

[44] Jan Sokolowski and Jean-Paul Zolésio. Introduction to shape optimization. In *Introduction to shape optimization*, pages 5–12. Springer, 1992.

[45] MTR Jayasinghe and WMVPK Jayasena. Effects of axial shortening of columns on design and construction of tall reinforced concrete buildings. *Practice periodical on structural design and construction*, 9(2):70–78, 2004.

[46] B Ali, Abdulazeez Rotimi, Shivan Tovi, Charles Goodchild, Joseph Rizzuto, et al. Evaluation of the influence of creep and shrinkage determinants on column shortening in mid-rise buildings. *Advances in Concrete Construction*, 5(2):155, 2017.

[47] Zenon A Zielinski, MS Troitski, and E El-Chakieh. Bearing capacity tests on precast concrete thin-wall ribbed panels. *Prestressed Concrete Institute Journal*, pages 89–103, 1983.

[48] Marlon Bazan and Chuck Oswald. Testing and analysis of precast concrete wall panels. In *16th International Symposium for the Interaction of the Effects of Munitions with Structures, Destin, FL*, 2015.

[49] Sarni H Rizkalla, Reynaud L Serrette, J Scott Heuvel, and Emmanuel K Attiogbe. Multiple shear key connections for precast shear wall panels. *PCI journal*, 34(2):104–120, 1989.

[50] Khaled A Soudki, Jeffrey S West, Sami H Rizkalla, and Bruce Blackett. Horizontal connections for precast concrete shear wall panels under cyclic shear loading. *PCI journal*, 41(3):64–80, 1996.

[51] Francisco J Crisafulli, José I Restrepo, and Robert Park. Seismic design of lightly reinforced precast concrete rectangular wall panels. *PCI journal*, 47(4):104–121, 2002.

[52] EN 1991-1-4. *Eurocode 1. Actions on structures - General actions - Wind actions*. European Committee for Standardization, London, 2005.

[53] NA SLS EN 1991-1-4: 2019. *Sri Lanka National Annex*

to Euro Code 1: Actions on Structures - Part 1 - 4: General Actions - Wind Actions. Sri Lanka Standards Institution, Colombo, Sri Lanka, 2019.

[54] EN 1993-1. *Eurocode 3: Design of steel structures - Part 1-1: General rules and rules for buildings.* European Committee for Standardization, London, 2005.